European Journal of Pharmaceutics and Biopharmaceutics 77 (2011) 353–359

Contents lists available at ScienceDirect

European Journal of Pharmaceutics and Biopharmaceutics

journal homepage: www.elsevier.com/locate/ejpb

Research paper

A shotgun proteomic study of the protein corona associated with cholesterol and atheronal-B surface-modified quantum dots

Kanlaya Prapainop [a], Paul Wentworth Jr. [a,b,*]

[a] Scripps-Oxford Laboratory, Department of Biochemistry, The University of Oxford, Oxford, United Kingdom
[b] Department of Chemistry, The Skaggs Institute for Chemical Biology, The Scripps Research Institute, CA, USA

ARTICLE INFO

Article history:
Available online 31 December 2010

Keyword:
Quantum dots
Protein corona
Oxysterols
Cholesterol
Nanoparticles
Proteomics

ABSTRACT

As part of ongoing research in our group, we are keen to monitor the protein binding and movement of sterols and oxysterols in biological systems in real time. However, prior to performing these *in vivo* studies, we have herein studied how sterol and oxysterol surface modification of quantum dots affects their associated protein coronas. Thus, we have synthesized and analyzed cholesterol and atheronal-B surface-modified quantum dots (termed QD-chol and QD-ath-B, respectively). The fluorescence properties and aggregation propensities of QD-chol and QD-ath-B are unchanged relative to amino-functionalized quantum dots (QD-NH_2) in aqueous buffers. Shotgun proteomic analyses of the protein coronas reveal that QD-ath-B and QD-chol are bound significantly higher to LDL, vLDL and HDL particles than QD-NH_2. Thus, almost all the component proteins of the HDL and LDL proteomes are elevated in the protein coronas around the QD-chol and QD-ath-B nanomaterials. In addition, the reduced positive surface charge of the QD-chol and QD-ath-B materials, relative to QD-NH_2, means that hydrophobic antibody light chain fragments and β-2-glycoprotein (apo H) bind them preferentially to QD-NH_2.

1. Introduction

Semiconductor nanocrystals, such as quantum dots, are increasingly being used both *in vitro* and *in vivo* because of their unique optical properties that overcome many of the existing limitations of conventional organic fluorophores. Specifically, quantum dots tend to have a broad excitation and narrow emission spectrum, which reduces signal overlap, thereby reducing quenching and improving sensitivity [1,2]. Quantum dots are also resistant to photobleaching; hence, they fluoresce for far longer periods than classical fluorophores [3]. In addition, quantum dots are resistant to metabolic degradation, consequently allowing for fluorescent emission in live cells for periods as long as two months [4]. In addition, the emission spectra of nanocrystals can be tuned by changing the size of the CdSe core, making these nanomaterials particularly useful. However, the real utility of quantum dots resides in the outer ZnS shell that can be modified with thiol-functionalized molecules, allowing surface modification by small molecules and biomolecules [5,6].

As the use of these materials in biological systems has increased, it has becoming important to understand their potential biological risks. As a composite of this, an understanding of nanoparticle–protein interactions is crucial to aid in the controlled development of these promising materials. As such, the interaction of gold nanoparticles with proteins in cell culture media containing 10% fetal bovine serum (FBS) has been investigated [7]. More recently, human plasma proteins and their interaction with a NIPAM-BAM copolymer, gold and surface-modified polystyrene derivatives, have revealed that both size and surface composition clearly influence the associated protein corona of nanoparticles [7–9].

Recent work in our laboratory has lead to the discovery of a new class of oxysterols *in vivo*, termed the atherenals. The atherenals are unique oxysterols derived from oxidative cleavage of cholesterol (**1**) at the 5–6 double bond giving aldehyde products, such as atheronal-B (**3**) (Fig. 1). These molecules (**3**) have been found in serum, atherosclerotic tissue and human brain tissue [10,11]. The atherenals are cytotoxic to cultured macrophage cells, monocyte differentiation and induce apo-B_{100} misfolding, all features considered relevant in atherogenesis [10]. We consider the adduction of these aldehydes-containing oxysterols to LDL a model for LDL-oxidation *in vivo*, and some of the biological effects of these compounds do mirror that of oxidized LDL (ox-LDL). For examples, ox-LDL can trigger the formation of lipid-laden macrophages called foam cells, which are the first observed pathological changes in atherosclerotic disease [10,12]. Arguably, the most significant effect of the atherenals is their ability to perturb the misfolding of many misfolding prone proteins, such as amyloid-β protein

* Corresponding author. Department of Chemistry (SR111), The Scripps Research Institute, 10550 N. Torrey Pines Rd., La Jolla, CA 92037, USA. Tel.: +1 858 7842576, +44 (0) 1865 285434; fax: +1 858 7847385, +44 (0) 1865 285329.
E-mail addresses: paulw@scripps.edu, paul.wentworth@bioch.ox.ac.uk (P. Wentworth).

0939-6411/$ - see front matter © 2010 Elsevier B.V. All rights reserved.
doi:10.1016/j.ejpb.2010.12.026

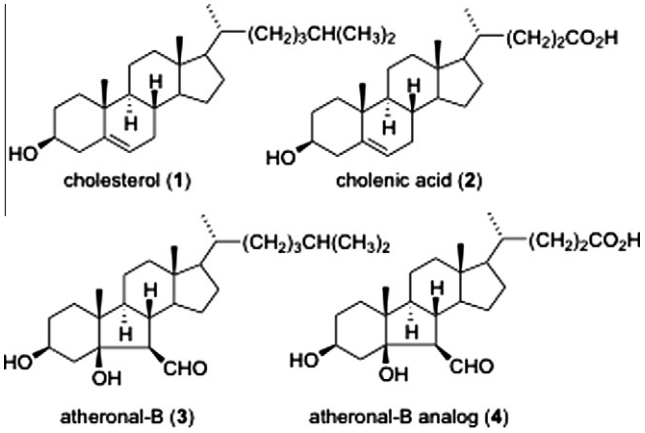

Fig. 1. Chemical structures of cholesterol (1), cholenic acid (2), atheronal B (3) and atheronal-B analog (4).

[11,13], α-synuclein [14], antibody light chains [15] and prion proteins [16].

At present, we have little information as to where these unique oxysterols are generated and how they may travel around the body. It seems reasonable that potential carriers for these oxysterols *in vivo* would be apolipoproteins, such as apo A, apo B, apo C, apo D apo E etc. that are themselves intrinsic protein components of HDL and LDL and that are involved in cholesterol, esterified and un-esterified and other lipid transport, including oxysterols [17]. A typical lipoprotein particle comprises of triglycerides and cholesterol esters in the core surrounded by the protein component and a monolayer of phospholipids. The lipoproteins are composites of different particles. For example, apo-B is the main component of LDL, whereas apo-A-I is the main component of HDL [18]. Apo-A-II and apo-E are enriched in sub-fractions of HDL, HDL_2 and HDL_3. However, the atheronals, which possess an aldehyde moiety, might reasonably bind to many and any additional proteins of the mammalian proteome *via* Schiff base adduction confounding a routine analysis of their potential carriers based purely on their lipid structure. Therefore, as a result of the important biological effects of these oxysterols and the difficulties in assessing the protein binding and movement of these compounds *in vivo* in real time, we have turned to quantum dots as traceable carriers for these aldehydes. In this preliminary study, we have prepared and analyzed quantum dots surface-modified with either cholesterol or atheronal-B and performed a shotgun proteomics study of their associated protein coronas after exposure to human plasma.

2. Materials and methods

All materials for chemical synthesis were purchased from Sigma–Aldrich (Dorset, UK) and used without further purification. Dichloromethane, ethyl acetate, methanol, chloroform, hexane and dimethylformamide were from Fisher Chemicals (Loughborough, UK). $CDCl_3$ was supplied by Cambridge Isotopes (Nantwich, UK). Qdot 585 ITK amino (PEG) was purchased from Invitrogen (Paisley, UK). Ultrafree-MC, PLTK Ultracel PL membrane Centrifugal Filter units (30 kDa) were from Millipore (Billerica, MA). Human plasma was purchased from HD supplies UK. All reactions were carried out in oven-dried glassware under an argon atmosphere with anhydrous solvents, unless otherwise noted.

2.1. Synthesis of atheronal B analog (**4**)

Aldehyde (**4**) was prepared in two steps from 5-cholenic acid-3β-ol (**2**) by modification of the method previously reported in our group [10]. Thus, 5-Cholenic acid-3β-ol (500 mg, 1.33 mmol) was dissolved in dichloromethane (45 mL) and methanol (5 mL), and the resultant solution was cooled to −78 °C in dry ice/acetone bath. A stream of O_2/O_3 was generated using an OL80 ozone generator (Ozonelab) and then passed through this stirred solution until the reaction was complete (*ca.* 1 h), followed by a stream of N_2 (g) for 20 min. The reaction mixture was allowed to warm to room temperature, and then resin-supported triphenylphosphine (3 mol/g resin) was added. The resultant mixture was allowed to stand overnight. The resin was then removed by filtration, and the filtrate was concentrated *in vacuo*. The mixture was then partitioned between H_2O (50 mL) and dichloromethane. The combined organic fractions were collected and dried over $MgSO_4$. The desiccant was removed by filtration, and the filtrate was evaporated *in vacuo*.

The ketoaldehyde intermediate **5** (266 mg, 0.56 mmol) was then dissolved in acetonitrile–water (20:1) 10 mL then stirred with L-proline (0.56 mmol) for 2 h at r.t. before concentrating *in vacuo* and being purified by silica gel chromatography (ethyl acetate: hexane 4:1). The atheronal B analog **4** was obtained as a white solid (88.7 mg, 57%). ^{1}H NMR ($CDCl_3$, 500 MHz) δ: 9.689 (d, J = 2.8 Hz, 1H), 4.115 (m, 1H), 3.565 (s,1H), 2.495 (broad s, 1H), 2.234 (dd, J = 9.2, 3.2 Hz, 1H), 0.920 (s, 3H), 0.904 (d, J = 6.4 Hz, 3H), 0.854 (d, J = 6.8 Hz, 3H), 0.850 (d, J = 6.8 Hz, 3H), 0.705 (s, 3H). ^{13}C NMR ($CDCl_3$) δ: 204.74, 84.26, 67.33, 63.89, 56.10, 55.67, 50.42, 45.47, 44.72, 44.22, 40.02, 39.67, 39.44, 36.15, 35.58, 28.30, 27.98, 27.91, 26.69, 24.55, 23.78, 22.78, 22.52, 21.54, 18.71, 18.43, 12.48. HR-MALDI-TOF-MS calcd for $C_{27}H_{46}O_3Na$ $(M + Na)^+$ 441.3339 found 441.3351. R_f = 0.4 (ethyl acetate/hexane 4:1).

2.2. Preparation of QD-chol (**7**) and QD-ath-B (**8**)

Ethyl(dimethylaminopropyl) carbodiimide (40 nmol), sulfo-NHS (40 nmol) and cholenic acid (**2**) or atheronal B analog (**4**) (40 nmol) were stirred in dimethylformamide (DMF, 50 μL) for 1 h at room temperature. Then, Qdot® 585 ITK™ amino (PEG) quantum dot ($QD-NH_2$) (0.4 nmol) (**6**) in borate buffer (pH 8.0, 100 μL) was added, and the resultant mixture was stirred over night at room temperature. The mixture was then exhaustively dialyzed against PBS [Ultrafree-MC, PLTK Ultracel PL membrane Centrifugal Filter units (30 kDa)] to give the modified QD-chol (**7**) or QD-ath-B dots (**8**).

2.3. Fluorescence spectroscopy

All fluorescence spectra of the nanomaterials were measured on a Molecular Devices M5 microtiter plate reader.

2.4. Hydrodynamic radius (HR) measurement

Quantum dot HRs were measured routinely by dynamic light scattering using a Viscotek DLS machine. Hydrodynamic radii were obtained from a mass-weight size distribution analysis and reported as the mean of triplicate measurements. Generally, DLS were performed within 24 h after initial preparation of all nanomaterials and immediately prior to any experiment including the TEM reported below. In general, all nanomaterials were essentially unchanged in terms of their apparent HR throughout the course of our studies.

2.5. Agarose gel electrophoresis

Electrophoresis of QDs was performed using a minicell Primo (Thermo) with 1% ultrapure agarose gel in 0.5 × TBE, pH 8.2 at 100 V for 50 min.

2.6. Zeta potential determinations

Nanoparticle zeta potentials were measured in PBS (pH 7.4) on a zeta-sizer Nano-ZS (Malvern Instrument Inc. Worcestershire, UK) with a 633 nm laser and analyzed using dispersion technology software 5.03.

2.7. Transmission electron microscopy (TEM)

TEM samples were prepared by placing a drop of colloidal dispersion of quantum dots in methanol onto a carbon-coated nickel grid (300 mesh) followed by natural evaporation of the solvent. Then, the TEM images were recorded with a JEOL 2000FX electron microscope.

2.8. Quantum dot incubation with human plasma

This procedure has been modified from a previous report [19]. In brief, quantum dots (0.1 nmol) in PBS (pH 7.5) were incubated in human plasma (280 μL) at 37 °C for 1 h. The samples were then centrifuged with at 50,000 rpm for 15 min to pellet the protein–quantum dot complexes. The pellet was washed with PBS (3×) to remove unbound and loosely bound protein complexes. The pellet was then suspended in SDS buffer and the resultant mixture heated to 90 °C for 5 min. The mixture was then centrifuged (13,000 rpm) for 5 min. The supernatant was then added to a 16% Tricine gel, but only run until the protein had penetrated the gel. Total protein was then excised and analyzed by mass spectrometry as detailed below. The experiment was performed in duplicate.

2.9. Protein analysis by shotgun proteomics

Total protein was in-gel digested with trypsin and analyzed by nanospray LC–MS/MS using a Thermo Orbitrap mass spectrometer coupled to a Dionex U3000 nano HPLC system. Data were analyzed for label free quantitation by Progenesis Software (NonLinear Dynamics Ltd.). Tryptic peptide sequences were identified by MASCOT software and matched to the international protein index IPI_human (TD) database v.3.64. Only proteins with a MASCOT score of >50 are reported.

3. Results and discussion

Preparation and physical properties of cholesterol and atheronal-B analog-surface-modified quantum dots atheronal-B analog **4** were synthesized in good yield using a modification of our previous procedure [10] and then coupled with qdot 585 amino (PEG) (**6**) in the presence of EDC and sulfo-NHS (Scheme 1). Simple dialysis afforded essentially homogeneous preparations of QD-ath-B (**8**) nanoparticle materials. Cholenic acid (**2**) was also conjugated to the amino-functionalized qdot 585 amino (PEG) (**6**) using the same EDC and sulfo-NHS method, to facilitate comparisons in protein surface binding between native cholesterol and the new class of oxysterols, the atheronals.

Fluorescence spectroscopy of the QD-ath-B and QD-chol nanomaterials in PBS revealed no measurable change in their fluorescence emission spectra relative to the parent QD-NH_2 (Fig. 2A). However, after conjugation of the hydrophobic sterol derivatives **2** and **4** with QD-NH_2, it is to be expected that the surface charge of these novel nanoparticles will be reduced relative to the untreated amino (PEG) nanoparticles. This was suggested qualitatively using agarose gel electrophoresis, which showed slightly increased migration toward the anode of the QD-ath-B and QD-chol nanoparticles relative to QD-NH_2 (Fig. 2B). This anode migration propensity was increased slightly with increasing amounts of functionalization **2** and **4** added during the conjugation process (0.5 eq. or 5.0 eq.). This change in surface charge was then quantified by measurement of ζ potential, which revealed that the QD-NH_2 that has ~100 amino groups per nanoparticle has a mean ζ potential of -2.66 ± 0.35 mV, which is decreased for the QD-chol (0.5 eq.) -3.21 ± 0.35 mV and QD-ath-B (0.5 eq.) -3.51 ± 0.28 mV and more so for QD-chol (5.0 eq.) -4.21 ± 0.38 mV and QD-ath-B (5.0 eq.) -4.73 ± 0.39 mV (Table 1). These ζ potential measurements confirm the agarose gel observations and show that as the number of free surface amino groups is reduced and is replaced by either **2** or **4**, the polarity is reduced, and hence, hydrophobicity is increased.

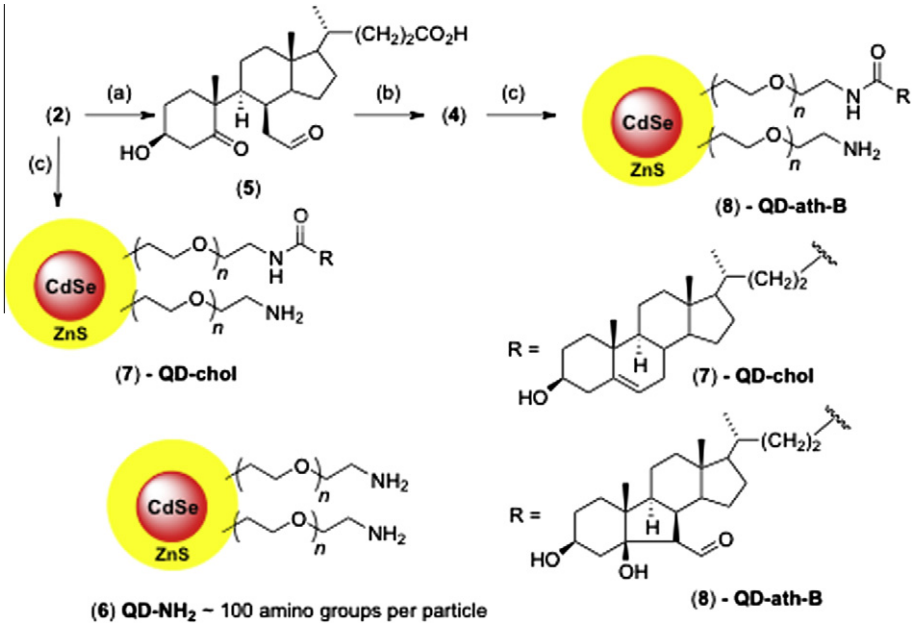

Scheme 1. Synthesis of cholenic acid analog quantum dots (QD-chol) and atheronal-B analog modified quantum dots (QD-ath-B): (a) (i) O_2/O_3, DCM:MeOH, −78 °C, 1 h (ii) PPh_3, r.t., overnight (b) L-Proline, r.t., 2 h (c) EDC, sulfo-NHS, r.t.

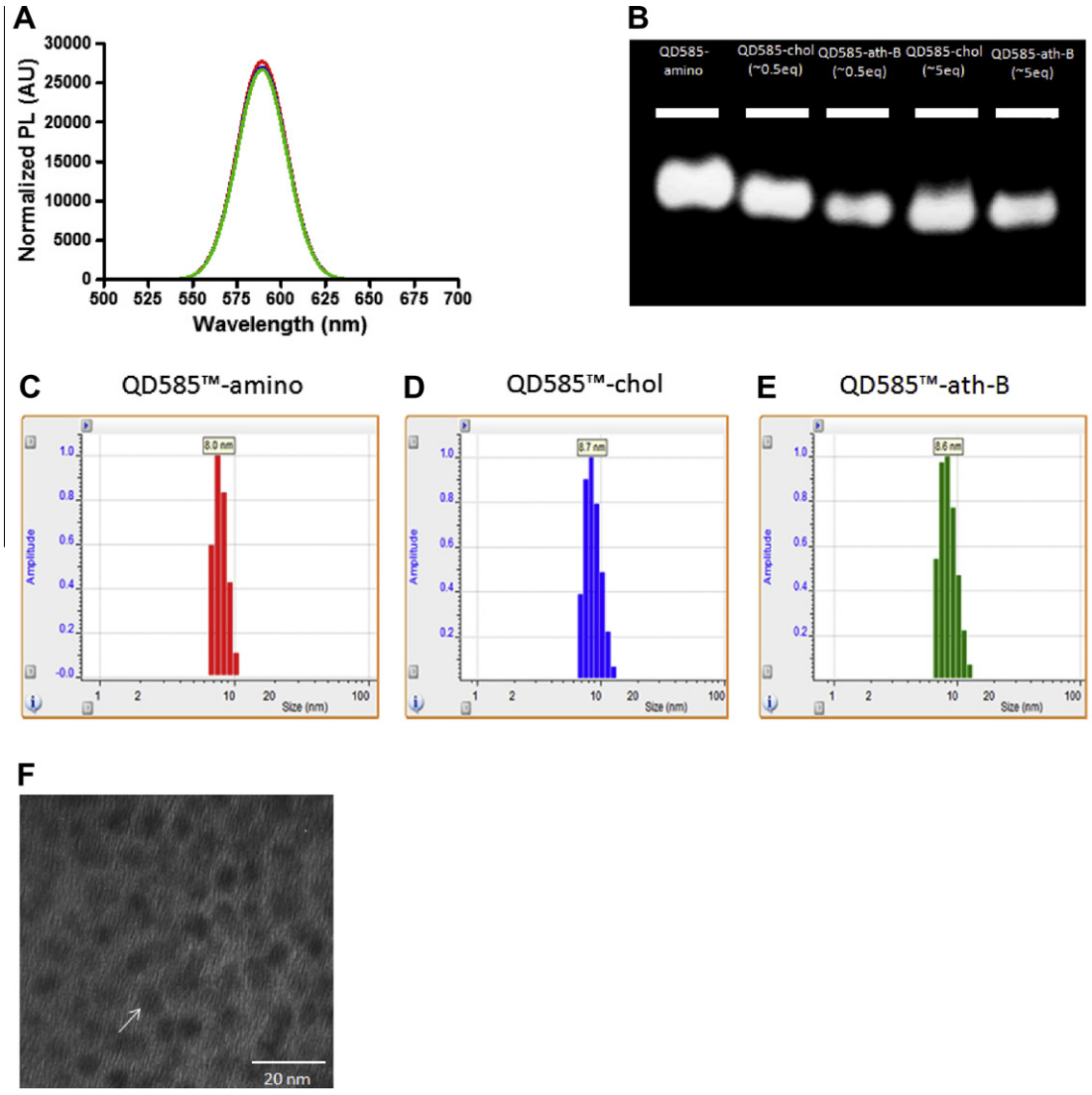

Fig. 2. Physical properties of cholesterol and atheronal-B modified quantum dots. (A) Normalized emission spectra of QD-NH_2 (red), QD-chol (blue) and QD-ath-B (green). (B) Gel shift modified quantum dots in 1% agarose gel buffered with Tris borate EDTA buffer (TBE, pH 8.2). Lane 1 QD-NH_2, lane 2 QD-chol (0.5 eq.), lane 3 QD-ath-B (0.5 eq.), lane 4 QD-chol (5 eq.) and lane 5 QD-ath-B (5 eq.). (C and E) Representative dynamic light-scattering histograms in PBS of C) QD-NH_2 (red) (D) QD-chol (blue) (E) QD-ath-B (green). F) TEM of QD-ath-B recorded on a JEOL 2000FX electron microscope. (For interpretation of the references to color in this figure legend, the reader is referred to the web version of this article.)

Table 1
Physical properties of quantum dots in this study.

Quantum dot type	Hydrodynamic radius (nm)	Zeta potential (mV)
QD-NH_2	7.92 ± 0.7	−2.66 ± 0.35
QD-chol (0.5 eq.)	7.15 ± 0.1	−3.21 ± 0.35
QD-ath-B (0.5 eq.)	7.45 ± 1.6	−3.51 ± 0.28
QD-chol (5.0 eq.)	8.82 ± 0.8	−4.21 ± 0.38
QD-ath-B (5.0 eq.)	8.51 ± 0.6	−4.73 ± 0.39

The reduction in nanomaterial charge when functionalized with **2** and **4**, an inescapable result of this specific surface chemistry, raised the concern that these particles may have a propensity to aggregate in aqueous buffers. However, dynamic light scattering studies, performed either immediately after nanomaterial preparation or for periods up to 6 months after preparation, revealed that the hydrodynamic radius (HR) of QD-ath-B (Fig. 2E) and QD-chol (Fig. 2D) are 8.51 ± 0.6 nm and 8.82 ± 0.8 nm, respectively, remaining unchanged in aqueous buffer with no evidence of higher HR aggregates being generated over time (the QDs-NH_2 have a measured HR of 7.92 ± 0.7 nm) (Fig. 2C). TEM analysis of QD-ath-B nanoparticles that have been in aqueous buffer for >3 months prior to the electron microscopy study, and that had been shown to have unchanged HR relative to immediately after preparation, shows discrete particles with a radius <10 nm, further supporting the notion that, although these novel oxysterol-coated particles have mean ζ potentials more negative than the untreated amino-functionalized nanomaterials, they do not appear to have a significantly increased propensity to aggregate in aqueous media up to 3 months (Fig. 2F).

3.1. Analysis of quantum dot surface protein association in human plasma

Human plasma contains over 3700 proteins, and they can associate with nanoparticles with different rate; some proteins might bind to particles rapidly when first exposed to biological fluids but dissociate rapidly to be replaced by other proteins that have slower exchange rates and higher affinity. In this study, we only consider tightly bound proteins components of the 'hard corona' because it has been considered the most relevant for an

understanding of nanoparticle–protein complexes that may interact with cells [20]. We analyzed the corona proteome by shotgun proteomics, an ideal method for direct analysis of a complex mixture [21].

A qualitative view of the hard corona profiles of QD-NH_2, QD-chol and QD-ath-B reveals the presence of a high number (>100) of the same proteins on all three nanomaterials (with a MASCOT score >50) (see Supporting information). However, the use of the Progenesis software package from NonLinear Dynamics allows relative protein abundances within proteomics data to be determined. Therefore, we have calculated the ratios of the abundances of each protein we find to be present on the QD-chol and QD-ath-B nanoparticles to the level observed on the amino-functionalized Qdot (Table 2).

Perhaps not surprisingly, the modified sterol and oxysterol surface-modified nanoparticles, QD-chol and QD-ath-B, are very much associated with a number of proteins involved with lipid and cholesterol transport and/or metabolism. The apolipoproteins with the highest ratios relative to QD-NH_2 being observed with the low-density lipoprotein (LDL)-associated protein apoB-100 (8.37 and 4.07, respectively) and the VLDL/HDL-associated protein apoC-III (9.11 and 6.04 respectively). Given that in each case the nanoparticle is coated with approximately the same molarity of sterol, the differences in protein binding should be related to the clearer simile of cholenic acid to cholesterol relative to the oxysterol atheronal

Table 2
[a,b]Ratio of proteins grouped according to their structure/function.

Protein	QD-chol/ QD-NH_2	QD-ath-B/ QD-NH_2
Lipid metabolism		
Apolipoprotein A-I	0.73	0.49
Apolipoprotein A-II	0.03	0.06
Apolipoprotein A-IV	1.69	1.70
Apolipoprotein B-100	8.37	4.07
Apolipoprotein C-I	0.29	0.33
Apolipoprotein C-II	1.29	0.05
Apolipoprotein C-III	9.11	6.04
Apolipoprotein C-IV	0.36	2.07
Apolipoprotein D	1.12	3.57
Apolipoprotein E	2.24	4.29
Apolipoprotein L1	0.60	5.85
Apolioprotein M	1.75	0.97
β-2-glycoprotein (apolipoprotein H)	2.58	4.41
Clusterin (apolipoprotein J)	9.53	7.96
Paraoxonase-1 (PON-1)	6.21	6.40
Complement pathway proteins		
Complement C1r	0.75	0.13
Complement C1q	0.79	1.30
Complement C1s	0.48	0.69
Complement C3	5.12	8.00
Complement C5	1.44	0.56
Plasma protease C1 inhibitor	7.43	4.32
Plasma serine protease inhibitor	12.46	8.23
Vitronectin	14.44	5.91
Acute-phase response proteins		
Inter-α trypsin inhibitor heavy chain H4	4.36	2.49
Serum amyloid A4	3.26	0.85
Transferrin	2.00	1.78
Lipopolysaccharide-binding protein	14.41	9.66
Proteinase inhibitors		
Haptoglobin-related protein	8.60	6.42
Angiotensinogen	11.26	6.96
Coagulation factors		
Fibronectin	0.71	0.42
Kininogen-1	10.30	9.17

[a] Ratios are of abundances of each protein, calculated using Progenesis, on either QD-chol or QD-ath-B relative to that of the amino-functionalized Qdot (QD-NH_2).
[b] For the full list of proteins/fragments detected in the protein coronas of these quantum dots see Supplementary information.

for these lipid-binding proteins. It should be stressed that the relative abundance of lipoproteins is not always highest with the sterol or oxysterol-coated nanoparticles. For example, apo A-I and A-II that are major components of sub-fractions of HDL particles show a lower abundance of binding to QD-chol and QD-ath-B (apo-A-I; 0.73, and 0.49, respectively, and Apo-A-II 0.03 and 0.06, respectively) relative to QD-NH_2. This low abundance of these two key HDL proteins is surprising considering that a high proportion of the known proteome of HDL and HDL sub-types [22,23] are present generally in higher abundance in the QD-chol and/or QD-ath-B protein coronas. For example, clusterin (Apo-J) [24], which is anti-inflammatory and promotes cholesterol efflux in HDL [25,26], shows a higher ratio of binding to both QD-chol and QD-ath-B. In addition, apo C-III, D, E, L-I (0.60 for QD-chol), M (0.97 for QD-ath-B), paraoxonase-1 (PON-1), serum amyloid A4 (SAA4), vitronectin, inter-α-trypsin inhibitor heavy chain H4, angiotensinogen, kininogen-1, serotransferrin, haptoglobin-related protein, complement protein C3 are all proteins known to be components of the HDL proteome and are all elevated in the coronas of the sterol and/or oxysterol coronas. Therefore, it seems to be the case that, in general, the sterol and oxysterol coating of the nanomaterials leads to association in plasma with VLDL, LDL and HDL particles and the majority of the proteome of these important lipid carrier assemblies. It has previously been shown that complete HDL lipoproteins are bound to large hydrophobic NIPAM/BAM copolymers (~200 nm diameter) [27], in a process thought to have been mediated by apo A-I. In our hands, it seems that apo A-I is not an important component of the binding of HDL to QD-chol and QD-ath-B nanomaterials because it has much reduced levels relative to other components of the proteome of these lipoprotein particles. This may be because of the surface coating by sterol and oxysterol that is guiding HDL binding, rather than apo A-I.

The protein coronas of the sterol- and oxysterol-coated nanomaterials also have elevated levels of lipopolysaccharide-binding protein (14.41 and 5.91 respectively) which is a composite of the innate immune system associated with apo A-I [28] and apo-B_{100} containing lipoproteins [29,30].

In addition to the association of the QD-chol and QD-ath-B with LDL, HDL and VLDL, these nanomaterials also bind preferentially to β-2-glycoprotein (ApoH), a protein linked to the binding of negatively charged foreign particles. ApoH has been shown to bind DNA [31] and other negatively charged phospholipids [32]; therefore, it has been proposed that one role for this plasma protein is to neutralize negatively charged macromolecules that enter the bloodstream and in doing so diminish unwanted activation of the blood coagulation [29]. Given the clear propensity this plasma protein has for negatively charged species, it is not a surprise that this protein binds to sterol and oxysterol modified quantum dots preferentially to QD-NH_2, which will be considerably more positively charged *in vivo*. In the same vein, there are elevated levels of certain antibody light chains, Ig κ V-1 and V-III regions chains in the corona of the less positively charged sterol and oxysterol (2.20, 2.37 and 2.81 and 2.96, respectively) relative to the QD-NH_2. Antibody domains are known to be hydrophobic and either self-associate or adhere to hydrophobic surfaces and so would be expected to associate preferentially with the sterol or oxysterol nanomaterials.

Previous reports have shown that nanoparticles of various size and composition are bound by complement protein fractions. This has lead to the assumption that nanoparticles may activate the complement system via the classical pathway as is observed with carbon nanotubes [33,34]. This makes sense, in that the classical pathway for complement activation requires the close proximity of Fc fragments of immunoglobulin proteins to trigger activation of C3. The nanoparticles, while much smaller than the surface of a bacterium, still possess a high local concentration of

immunoglobulins as a result of their corona and as such may well trigger complement activation. What this study shows is that there can be considerably different amounts of the complement proteins on different nanoparticles (Table 2). Thus, while the levels of C1q and C1s are elevated in the QD-NH_2 corona, the levels of C3, plasma protease C1 inhibitor and plasma serine protease inhibitor are all much higher on the sterol-modified nanoparticles. The complement protein C3 and plasma protease C1 and serine protease inhibitors in complex with vitronectin and clusterin have all been shown to be composites of the HDL proteome [30]. Therefore, the elevated levels of these specific proteins cannot be ascribed to any complement pathway activation by the nanomaterials. However, the presence of the complement protein fragments in the QD-NH_2 corona, without the additional components of the HDL proteome, suggests that nanomaterial-linked complement activation may be occurring in this case. These differences hint at different levels of complement activation/inhibition as a function of nanoparticle surface composition further complicating our understanding of what may happen when these materials are introduced *in vivo*.

4. Conclusions

In this study, we have prepared cholesterol and atheronal-B surface-modified quantum dots of well defined composition and possessing physical properties, such as fluorescence emission, and HR virtually indistinguishable from untreated amino (PEG) quantum dots from which they are derived. Exposure of these quantum dots to human plasma leads to the establishment of a 'hard corona' whose composition is dependent upon whether the surface modification is cholesterol or atheronal-B and which is replete with apolipoproteins and HDL/LDL/vLDL proteomes and proteins of the complement system. The absolute amounts of the proteins in these coronas are quite often significantly higher or lower than amino surface PEG quantum dots, showing that the surface modification with sterols and oxysterols clearly perturbs the protein corona of these nanomaterials in a way that reflects the interactions between these molecules and their native carriers *in vivo*. For the next phase of our studies, cell based experiments, we will determine the soft or outer corona proteome that will then interact with cell surface receptors. It is now our hope that these particles can be used as traceable probes of sterol and oxysterol protein binding for cellular and *in vivo* studies.

Acknowledgements

This work was supported by a grant from The Scripps Research Institute and The Skaggs Institute for Chemical Biology to P.W. K.P. acknowledges the support of a Royal Thai Government Post Graduate Scholarship. The authors would also like to thank Dr. Benjamin Thomas, of the Proteomics Facility, Sir William Dunn Pathology School, for assistance with the proteomic studies, the Computational Biology Research Group, Medical Sciences Division, Oxford, for assistance with data mining, and Dr. Karaked Tedsree of the Inorganic Chemistry Department, for assistance with the TEM analyses.

Appendix A. Supplementary material

Supplementary data associated with this article can be found, in the online version, at doi:10.1016/j.ejpb.2010.12.026.

References

[1] J.K. Jaiswal, S.M. Simon, Potentials and pitfalls of fluorescent quantum dots for biological imaging, Trends Cell Biol. 14 (2004) 497–504.
[2] W.J. Parak, T. Pellegrino, C. Plank, Labelling of cells with quantum dots, Nanotechnology 16 (2005) R9–R25.
[3] X. Michalet, F.F. Pinaud, L.A. Bentolila, J.M. Tsay, S. Doose, J.J. Li, G. Sundaresan, A.M. Wu, S.S. Gambhir, S. Weiss, Quantum dots for live cells, in vivo imaging, and diagnostics, Science 307 (2005) 538–544.
[4] B. Ballou, B.C. Lagerholm, L.A. Ernst, M.P. Bruchez, A.S. Waggoner, Noninvasive imaging of quantum dots in mice, Bioconj. Chem. 15 (2004) 79–86.
[5] E. Casals, T. Pfaller, A. Duschl, G.J. Oostingh, V. Puntes, Time evolution of the nanoparticle protein corona, ACS Nano 4 (2010) 3623–3632.
[6] I.L. Medintz, H.T. Uyeda, E.R. Goldman, H. Mattoussi, Quantum dot bioconjugates for imaging, labelling and sensing, Nat. Mater. 4 (2005) 435–446.
[7] S.H.D.P. Lacerda, J.J. Park, C. Meuse, D. Pristinski, M.L. Becker, A. Karim, J.F. Douglas, Interaction of gold nanoparticles with common human blood proteins, ACS Nano 4 (2009) 365–379.
[8] T. Cedervall, I. Lynch, M. Foy, T. Berggård, Seamas C. Donnelly, G. Cagney, S. Linse, Kenneth A. Dawson, Detailed identification of plasma proteins adsorbed on copolymer nanoparticles, Angew. Chem. Int. Ed. 46 (2007) 5754–5756.
[9] M. Lundqvist, J. Stigler, G. Elia, I. Lynch, T. Cedervall, K.A. Dawson, Nanoparticle size and surface properties determine the protein corona with possible implications for biological impacts, Proc. Nat. Acad. Sci. USA 105 (2008) 14265–14270.
[10] P. Wentworth Jr., J. Nieva, C. Takeuchi, R. Galve, A.D. Wentworth, R.B. Dilley, G.A. DeLaria, A. Saven, B.M. Babior, K.D. Janda, A. Eschenmoser, R.A. Lerner, Evidence for ozone formation in human atherosclerotic arteries, Science 302 (2003) 1053–1056.
[11] Q. Zhang, E.T. Powers, J. Nieva, M.E. Huff, M.A. Dendle, J. Bieschke, C.G. Glabe, A. Eschenmoser, P. Wentworth Jr., R.A. Lerner, J.W. Kelly, Metabolite-initiated protein misfolding may trigger Alzheimer's disease, Proc. Nat. Acad. Sci. USA 101 (2004) 4752–4757.
[12] C. Takeuchi, R. Galve, J. Nieva, D.P. Witter, A.D. Wentworth, R.P. Troseth, R.A. Lerner, P. Wentworth Jr., Proatherogenic effects of the cholesterol ozonolysis products, atheronal-A and atheronal-B, Biochemistry 45 (2006) 7162–7170.
[13] J.C. Scheinost, H. Wang, G. Boldt, J. Offer, P. Wentworth Jr., Cholesterol secosterol-induced aggregation of methylated amyloid-beta peptides – insights into aldehyde-initiated fibrillization of amyloid-beta, Angew. Chem. Int. Ed. 47 (2008) 3919–3922.
[14] D.A. Bosco, D.M. Fowler, Q. Zhang, J. Nieva, E.T. Powers, P. Wentworth Jr., R.A. Lerner, J.W. Kelly, Elevated levels of oxidized cholesterol metabolites in Lewy body disease brains accelerate alpha-synuclein fibrilization, Nat. Chem. Biol. 2 (2006) 249–253.
[15] J. Nieva, A. Shafton, L.J. Altobell, S. Tripuraneni, J.K. Rogel, A.D. Wentworth, R.A. Lerner, P. Wentworth, Lipid-derived aldehydes accelerate light chain amyloid and amorphous aggregation, Biochemistry 47 (2008) 7695–7705.
[16] J.C. Scheinost, D.P. Witter, G.E. Boldt, J. Offer, P.J. Wentworth, Cholesterol secosterol adduction inhibits the misfolding of a mutant prion protein fragment that induces neurodegeneration, Angew. Chem. Int. Ed. 48 (2009) 9469–9472.
[17] R.W. Mahley, T.L. Innerarity, S.C. Rall, K.H. Weisgraber, Plasma lipoproteins: apolipoprotein structure and function, J. Lipid Res. 25 (1984) 1277–1294.
[18] P. Alaupovic, Apolioproteins and lipoproteins, Atherosclerosis 13 (1971) 141–146.
[19] I. Lynch, T. Cedervall, M. Lundqvist, C. Cabaleiro-Lago, S. Linse, K.A. Dawson, The nanoparticle–protein complex as a biological entity; a complex fluids and surface science challenge for the 21st century, Adv. Colloid Interf. Sci. 134–135 (2007) 167–174.
[20] I. Lynch, T. Cedervall, M. Lundqvist, C. Cabaleiro-Lago, S. Linse, K.A. Dawson, The nanoparticle–protein complex as a biological entity; a complex fluids and surface science challenge for the 21st century, Adv. Colloid Interf. Sci. 134–135 (2007) 167–174.
[21] E.M. Marcotte, How do shotgun proteomics algorithms identify proteins?, Nat Biotechnol. 25 (2007) 755–757.
[22] H.V. de Silva, W.D. Stuart, C.R. Duvic, J.R. Wetterau, M.J. Ray, D.G. Ferguson, H.W. Albers, W.R. Smith, J.A. Harmony, A 70-kDa apolipoprotein designated Apo J is a marker for subclasses of human plasma high density lipoproteins, J. Biol. Chem. 265 (1990) 13240–13247.
[23] D.E. Jenne, J. Tschopp, Clusterin: the intriguing guises of a widely expressed glycoprotein, Trends Biochem. Sci. 17 (1992) 154–159.
[24] I.C. Gelissen, T. Hochgrebe, M.R. Wilson, S.B. Easterbrook-Smith, W. Jessup, R.T. Dean, A.J. Brown, Apolipoprotein J (clusterin) induces cholesterol export from macrophage-foam cells: a potential anti-atherogenic function?, Biochem J. 331 (1998) 231–237.
[25] J. Krøll, J.K. Larsen, H. Loft, M. Ezban, K. Wallevik, M. Faber, DNA-binding proteins in Yoshida ascites tumor fluid, Biochim. Biophys. Acta 434 (1976) 490–501.
[26] J.S. Liang, J.D. Sipe, Recombinant human serum amyloid A (apoSAAp) binds cholesterol and modulates cholesterol flux, J. Lipid Res. 36 (1995) 37–46.
[27] E. Hellstrand, I. Lynch, A. Andersson, T. Drakenberg, B. Dahlback, K.A. Dawson, S. Linse, T. Cedervall, Complete high-density lipoprotein in nanoparticle corona, FEBS 276 (2009) 3372–3381.
[28] H.P. McNeil, R.J. Simpson, C.N. Chesterman, S.A. Krilis, Anti-phospholipid antibodies are directed against a complex antigen that includes a lipid-binding inhibitor of coagulation: beta 2-glycoprotein I (apolipoprotein H), Proc. Nat. Acad. Sci. USA 87 (1990) 4120–4124.

[29] I. Schousboe, Beta 2-glycoprotein I: a plasma inhibitor of the contact activation of the intrinsic blood coagulation pathway, Blood 66 (1985) 1086–1091.
[30] T. Vaisar, S. Pennathur, P.S. Green, S.A. Gharib, A.N. Hoofnagle, M.C. Cheung, J. Byun, S. Vuletic, S. Kassim, P. Singh, H. Chea, R.H. Knopp, J. Brunzell, R. Geary, A. Chait, X.-Q. Zhao, K. Elkon, S. Marcovina, P. Ridker, J.F. Oram, J.W. Heinecke, Shotgun proteomics implicates protease inhibition and complement activation in the antiinflammatory properties of HDL, J. Clin. Invest. 117 (2007) 746–756.
[31] J.W. Heinecke, The HDL proteome: a marker – and perhaps mediator – of coronary artery disease, J. Lipid Res. 50 (2009) S167–S171.
[32] R.C. Wiggins, B.N. Bouma, C.G. Cochrane, J.H. Griffin, Role of high-molecular-weight kininogen in surface-binding and activation of coagulation Factor XI and prekallikrein, Proc. Nat. Acad. Sci. USA 74 (1977) 4636–4640.
[33] C. Salvador-Morales, E. Flahaut, E. Sim, J. Sloan, M.L. Green, R.B. Sim, Complement activation and protein adsorption by carbon nanotubes, Mol. Immunol. 43 (2006) 193–201.
[34] C. Salvador-Morales, E. Flahaut, E. Sim, J. Sloan, M.L.H. Green, R.B. Sim, Complement activation and protein adsorption by carbon nanotubes, Mol. Immunol. 43 (2006) 193–201.